Immobilising ruthenium organosilane complexes on ITO electrode surface towards electrogenerated chemiluminescence.

F. Mayorga[1,3], R.A. Fernández [1,3], C.I. Vázquez[1,3], J.E. Argüello[2,3,*], F.P. Cometto[1,3], S.A. Dassie[1,3,*]

[1]Universidad Nacional de Córdoba. Facultad de Ciencias Químicas. Departamento de Fisicoquímica. Ciudad Universitaria. X5000HUA. Córdoba. Argentina.

[2]Universidad Nacional de Córdoba. Facultad de Ciencias Químicas. Departamento de Química Orgánica. Ciudad Universitaria. X5000HUA. Córdoba. Argentina.

[3]Instituto de Investigaciones en Fisicoquímica de Córdoba (INFIQC), CONICET. Ciudad Universitaria. X5000HUA. Córdoba. Argentina.

Abstract

A light-emitting organosilane molecule based on a Ru-complex was synthesized from 1,10-phenanthroline, (3-Aminopropyl)triethoxysilane (APTES), ruthenium trichloride, and 2,2′-Bipyridine. The resulting complex was covalently attached to a transparent conductive substrate, Indium-Tin Oxide (ITO), using a straightforward dipping method. Surface characterization of the modified substrates was conducted through X-ray photoelectron spectroscopy (XPS) and electrochemical experiments, confirming the presence of covalent bonds. The immobilized film of the ruthenium organosilane complex on ITO demonstrated robust stability as a modified electrode and holds significant promise as a novel light-emitting material.

Keywords: light-emitting molecule, ruthenium organosilane complex, electrogenerated chemiluminescence.

[*]Corresponding authors: *e-mail address*: J.E. Argüello (juan.arguello@unc.edu.ar) and S.A. Dassie (sadassie@unc.edu.ar)

1. Introduction

Electrogenerated chemiluminescence, or electrochemiluminescence (ECL), refers to the production of light from excited states generated by electrochemically induced electron transfer reactions [1,2] One method of generating excited states in ECL involves the use of a co-reactant. A co-reactant is a species that, upon oxidation or reduction, produces an intermediate capable of reacting with an ECL luminophore to produce excited states. It is widely reported in the literature that oxidation of $\left[\mathrm{Ru(bpy)_3}\right]^{2+}$ (where bpy refers to 2,2'-bipyridine) in the presence of tri-*n*-propylamine (TPA) leads to light emission similar to that produced by photoexcitation [3–5]. This is the most frequently used co-reactant in ECL systems, and its mechanism has been extensively explored by numerous research groups worldwide [4,6–14]. In the co-reactant approach [3,8,15], a species present in the solution (TPA) is oxidized within the same potential range as the luminophore ($\left[\mathrm{Ru(bpy)_3}\right]^{2+}$) species. Through electron transfers or subsequent chemical reactions following electron transfer, the co-reactant generates a product that reacts with the luminophore $\left[\mathrm{Ru(bpy)_3}\right]^{2+}$ species to generate an excited state ($\left[\mathrm{Ru(bpy)_3}\right]^{2+*}$) [14]. The versatility demonstrated by the chemiluminescent reaction of ruthenium complexes in solution has resulted in its widespread application for the determination of different species. However, a significant drawback of this ECL reaction is the need to constantly supply the reagent to the reaction site. An alternative to this involves the use of species adsorbed on different conductive substrates. In recent years, the field of electrochemistry related to modified electrodes has made significant advancements, thanks to the progress in self-assembled monolayers and nanoscience applied to the production of various electronic devices [16]. Since the pioneering works of Prof. Bard and co-workers [6,8,15,17–24], a variety of immobilization methods on the electrode surface with different degrees of difficulty have been developed up to the present, yielding diverse levels of success [16,25,26]. Evidently, a solid-state electroluminescent device with immobilized molecules that can act as a probe on its surface can reduce the consumption of expensive reactants and also enhance its portability and reutilization [25,27–31]. The immobilization of molecules onto a surface is critical for preventing probe leakage from the surface when it is used as a detector. Therefore, different approaches have been developed by changing the deposition methods on different surfaces, including gold [32,33], silica [25,27,31,34] and ITO [35,36].

In this study, we synthesized an organic light-emitting molecule based on a Ru-complex to subsequent covalent linking it to ITO electrodes. Structural characterization of the modified electrode was conducted using X-ray photoelectron spectroscopy (XPS). The electrochemical

properties of the modified electrode were investigated via cyclic voltammetry (CV), while the stability of the adducts under various experimental conditions was explored using XPS and CV. Finally, the ITO substrate modified with the ruthenium complex, in the presence of TPA as a co-reactant, was successfully tested as a light emitter.

2. Materials and Methods

2.1 Materials

Starting materials and solvents were purchased from Sigma-Aldrich and used as received. ITO (indium tin oxide)-coated glasses (float glass cuvette slides 7 mm × 50 mm × 0.9 mm, sheet resistance = 8 - 12 Ω sq^{-1}) were purchased from Delta Technologies.

2.2 Pretreatment of the ITO surface and Immobilization of Ru-Complex

ITO substrates were pretreated by washing steps in an ultrasonic bath for 5 minutes each, with the following sequence of solvents: acetone, ethanol, and ultrapure deionized water (Milli-Q, Millipore, 18.2 MΩ cm) and dried under flowing N_2 gas. Afterward, a modified RCA cleaning treatment [37,38] was used, by immersing the substrates in H_2O_2:NH_4OH:H_2O 1:1:5 mixture (in volume) at 65 ºC for 1 hour. The activated ITO surface was dried with N_2 gas and immersed in a 0.5 mg mL^{-1} Ru-Complex (**Complex 4**) solution with 0.2 M H_2SO_4, for 30 minutes. Finally, the treated ITO was washed with acetone in an ultrasonic bath for 30 s and dried with N_2 gas, to obtain the functionalized surface.

2.3 Mass spectrometry

Mass spectrometry spectra were measured in a Waters Spectrometer, model Xevo TQ-S by the following conditions: Direct infusion: 5 µL min^{-1}. Polarity: Positive Mode. Capillary voltage: 2.0 kV. Cone voltage: 10 V. Source temperature: 150 ºC. Desolvation temperature: 200 ºC. Desolvation gas: Nitrogen (300 L/h). Collision gas: Argon. Mass range between 50-1500 Daltons. Scan time: 1 second. Acquisition time: 2 minutes.

2.4 X-ray photoelectron Spectroscopy (XPS)

XPS measurements were performed with a Thermo Scientific K-Alpha+ X-ray Photoelectron Spectrometer. Spectra were recorded at room temperature, using non-monochromatized Al-K (1200 W) radiation for excitation and a 180 double-focus hemispherical analyser in a vacuum of 10 mbar. The diameter of the sampling area was 300 µm. The overall energy resolution for all the experiments was 0.05 eV, and the binding energy scale of the systems was calibrated using C1s = 284.8 eV from PET (polyethylene terephthalate) samples.

2.5 Cyclic voltammetry

Electrochemical experiments were carried out using a commercial potentiostat-galvanostat (Autolab PGSTAT100) in the conventional three-electrode setup, using the NOVA 1.10 software

package. Before each experiment, bare ITO and **ITO:4** working electrodes were rinsed with Milli-Q water and dried at room temperature. Platinum and silver wires were used as counter and quasi-reference electrodes, respectively. All experiments were performed at room temperature and dark environment, employing a polytetrafluoroethylene (PTFE) cell. Exposed working electrode area to the electrolyte was equal to 0.19 cm^2.

2.6. Electrogenerated chemiluminescence measurement

The determination of the electrogenerated chemiluminescence (ECL) of this modified substrate (**ITO:4**) was carried out, using TPA as a co-reactant. To do this, the **ITO:4** substrate was immersed in a solution of 1.0 mM TPA in 0.1 M $NaClO_4$ in acetonitrile, exposing an approximate area of 1.2 cm^2. The response was analysed for a potential sweep scan rate of 5.000 Vs^{-1} from 0.6 to 1.8 V vs Ag. A platinum wire was used as a counter-electrode and silver wire as a quasi-reference electrode. A Hamamatsu R928 photomultiplier (PMT), powered by a 900 V continuous source, was used to capture the electrogenerated light. The PMT was connected to a transimpedance amplifier, to record the signal using a tds3000 oscilloscope.

3. Results and discussion

3.1 Synthesis and Characterization of Ru-complex.

The synthesis of the Ru-Complex intended for attachment to the ITO surface (referred to as **Complex 4**) is elaborately described in the Supporting Information and depicted graphically in Scheme 1. In summary, 3,3′-dinicothinic acid (Compound **1**) was obtained through the oxidation of 1,10-phenantroline with $KMnO_4$, following the method developed by Kanungo *et al.* [39]. Subsequently, utilizing N,N'-dicyclohexylcarbodiimide (DCC) as an activating agent, the amide bond formation between the carboxylic group of Compound **1** and 3-aminopropyl)triethoxysilane (APTES) yielded Compound **2** (Scheme 1, Reaction (1); further synthesis details can be found in Ref. [40]). Di-(2,2'-bipyridyl) ruthenium dichloride (referred to as Complex **3**) was synthesized according to the procedure outlined in Ref. [41]. Finally, **Complex 4** was obtained by dissolving Compound **2** and Complex **3** in absolute ethanol and stirring the mixture at 50 ºC for 48 hours (Scheme 1, Reaction (2)) [27]. Upon dissolution in water, the synthesized Complex **3** and **4** generated a red-coloured solution with good solubility, while Compound **2** solutions exhibited a soft yellow colour. Mass spectrometry analysis was performed on all these compounds (refer to Fig. SI.1). **Complex 4** exhibited a signal at 532 m/z, corresponding to the expected complex's molecular weight. The ion with 532 m/z can be attributed to **Complex 4** after the loss of two Cl^- counteranions, displaying its characteristic Ruthenium isotopic mass distribution, as observed.

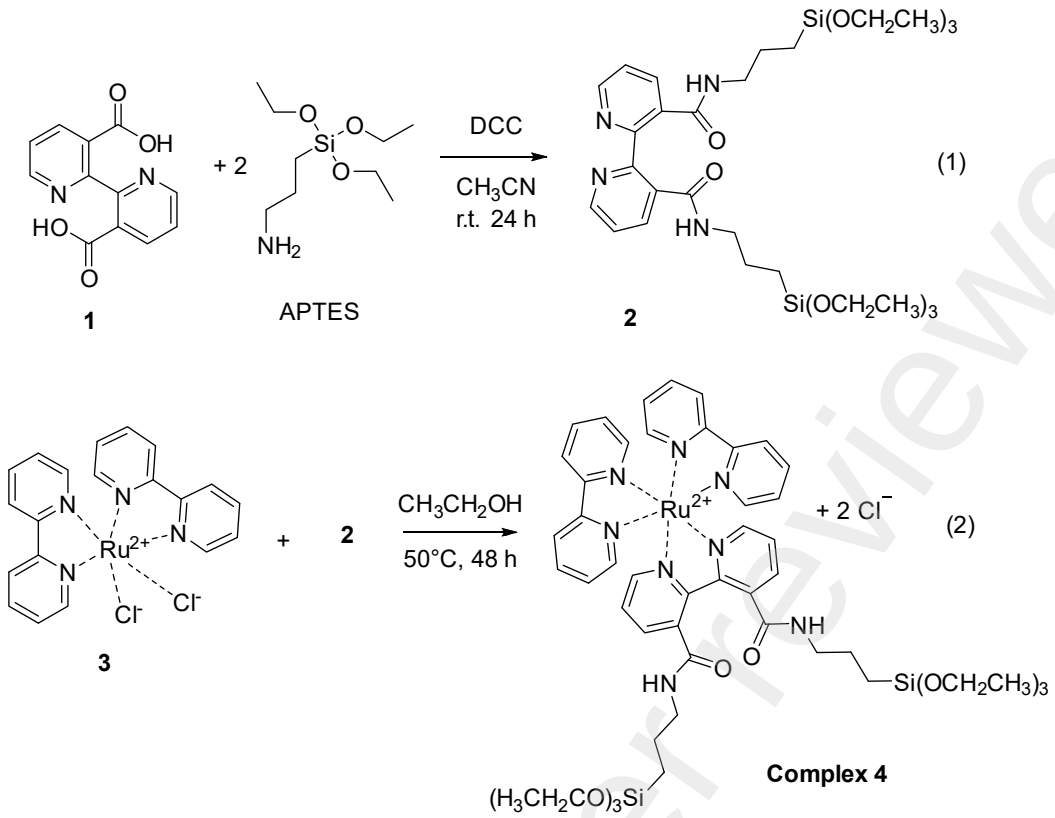

Scheme 1: Illustrative representation of the synthesis of **Complex 4**

In order to investigate the composition and the chemical environment of the synthesized Complexes **3** and **4**, an extensive X-ray photoelectron spectroscopy (XPS) analysis was conducted. This method is highly effective in furnishing both qualitative and quantitative data on the surface chemistry of a sample. The XPS survey spectra for Complexes **3** and **4** are depicted in Fig. 1 (a) and (b), respectively. Upon analysing the survey spectra of Complex **3**, it is evident that the presence of C, N, and Cl atoms can be readily identified by observing the peaks of photoelectrons that were ejected from the C1s (~285 eV), N1s (~400 eV), and Cl2p (~198 eV) states, respectively. Although the Ru3d peaks may be overlapped by the C1s peak, the existence of Ru species in the survey can still be discerned by the prominent Ru3p doublet at approximately 462 eV. As anticipated, the absence of Si and the relatively low quantity of O signifies the high purity of Complex **3**. Conversely, in **Complex 4**, the relative amount of C and O increases, along with the emergence of a Si2p peak at 102.5 eV that is attributed to Si from organosilanes environments (inset in panel (b) in Fig. 1) [42]. Fig. 1 (c) and (d) show the XPS spectra in the usual C1s region. As it was pointed out before, Ru3d signals are overlapped with C1s features [43]. Nevertheless, a prominent signal can be detected at the 280.8 – 281.2 eV range that are attributed to the Ru3d 5/2 signal.

The XPS spectra of Complexes **3** and **4** (depicted in Fig. 1 (c) and (d)) were subject to analysis in the region of the Ru3d core-level peak, which, as it was previously mentioned, partly overlaps with the C1s core-level peak. The Ru spectrum consists of two peaks that correspond to the spin-orbit split 3d 5/2 and 3d 3/2, whose positions vary depending on the oxidation state and chemical environment. The spectra can be interpreted as a convolution of the contribution from 4 well-defined peaks of carbon (1s), along with a split peaks for Ru, utilizing an asymmetric Voigt function for each Ru3d peak (as delineated by Morgan [43]), as well as a Shirley-type background. According to bibliography, the doublet at 280.8 eV and 284.9 eV can be assigned to Ru^{2+} species and it is compatible with the presence of coordinated Ru^{2+} in Compound **2** [33,35]. The main C1s core-level peak (located at 284.8 eV) can be assigned to both C atoms from aromatic rings and adventitious carbon. Furthermore, there exist three minor contributions to the C1s convolution that are ascribed to oxidized C species (C-O, C=O, and COOH) at 286.3 eV, 287.7 eV, and 289.4 eV, respectively. These may have resulted from impurities in the sample, possibly from manipulation and preparation of the sample prior to its introduction into the XPS vacuum chamber. Conversely, in the case of **Complex 4**, all the C1s components display an increase, which can be attributed to the inclusion of the aliphatic carbon skeleton, as well as carbon atoms that are bonded to O (R-C*-O-Si). Another distinction observed in the XPS spectrum of **Complex 4** is that the fitting procedure proposes the integration of an additional set of Ru3p peaks (279.9 eV/284.7 eV), which corresponds to a Ru^{2+} in a distinct environment, such as in **Complex 4**. The previous set of peaks, on the other hand, is still present and could be attributed to the presence of Complex **3** due to incomplete synthesis, as also identified in the mass spectroscopy analysis (Fig. SI.1).

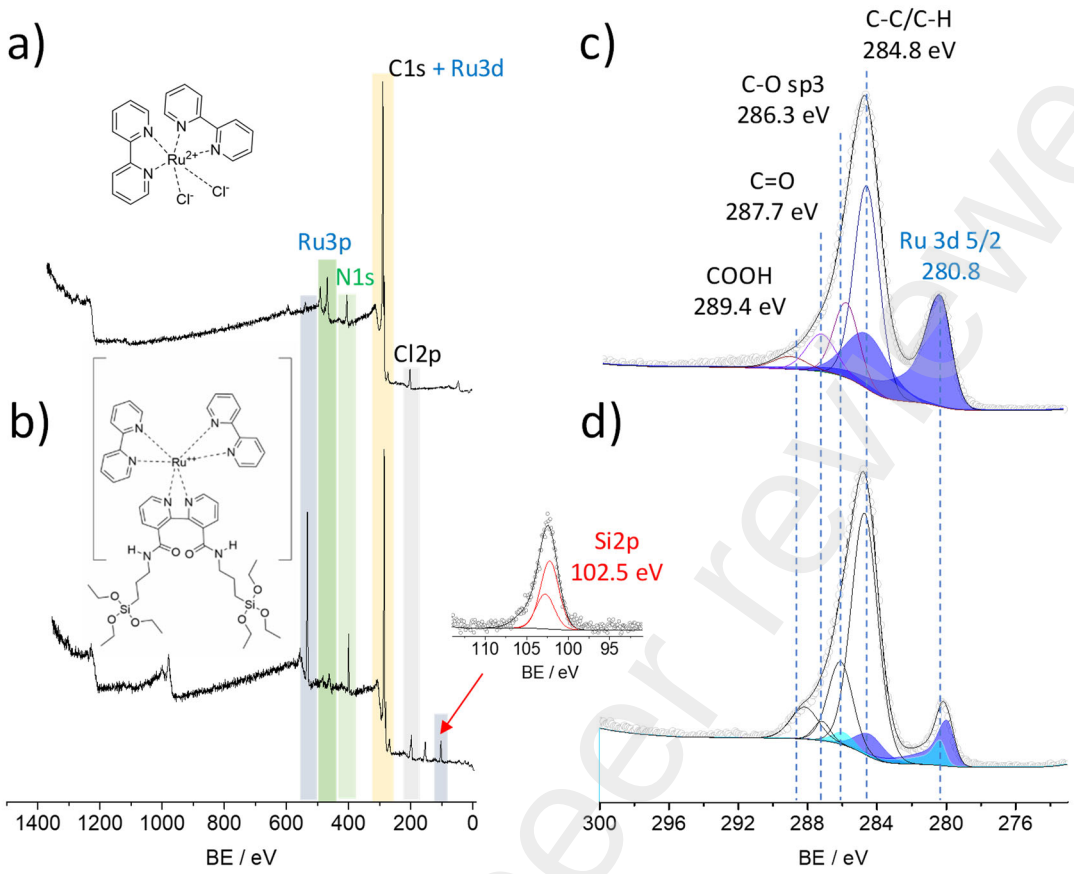

Figure 1: Survey and C1s-Ru3d core-level XPS spectra of Complex **3** (a) and (c) and **Complex 4** (b) and (d), respectively.

3.2 Immobilization of Complex 4 onto the ITO surface

Before being exposed to **Complex 4**, the ITO surface undergoes thorough washing and activation using the RCA solution. This treatment results in an increase in the number of OH groups, as indicated by the O1s signal in the XPS spectra (refer to Fig. SI.2) [44]. This increment plays a critical role in facilitating chemical interaction between the substrate and siloxane groups. Subsequently, the activated ITO surface was dried with N_2 gas and then immersed for 30 minutes in a 0.2 M H_2SO_4 solution containing **Complex 4** (0.5 mg mL^{-1}) to facilitate covalent bonding between the complex and the ITO surface, yielding **ITO:4**. Once **Complex 4** was immobilized on the surface as depicted in Scheme 2, the **ITO:4** substrate was subjected to analysis via cyclic voltammetry and XPS measurements.

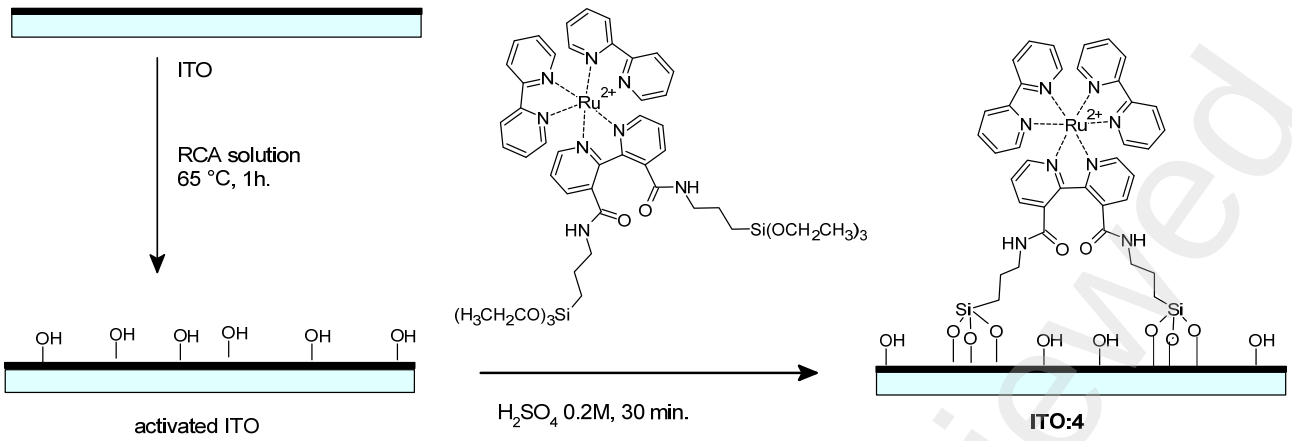

Scheme 2: Illustrative representation of immobilization of **Complex 4** on activated ITO surface (**ITO:4**)

To examine the electrochemical behaviour of the Ru-complex immobilized on a conductive surface, cyclic voltammograms of **ITO:4** samples were conducted (refer to Fig. 2). Fig. 2(a) illustrates characteristic cyclic voltammograms (at a scan rate of 4.000 Vs^{-1}) of both the **ITO:4** sample and the bare ITO surface. It is evident that there are no indications of faradaic current on the bare ITO surface (represented by the violet line). On the other hand, the **ITO:4** substrate exhibits a pair of redox signals at approximately 1 V vs Ag, which can be attributed to Ru(III)/Ru(II) redox couple [45] present in the **Complex 4** attached to the ITO conductive surface. When **ITO:4** undergoes several cycles of scanning, a reduction in the faradaic current is observed, after the first cycle until the signal becomes constant at the 6th cycle (orange line). Next, **ITO:4** was evaluated for subsequent cycles after the sixth cycle, at 4.000 Vs^{-1} keeping the signal constant. After measuring cyclic voltammograms at different scan rates, a linear relationship between the scan rate and the anodic current peak is observed (as it is shown in the inset of Fig. 2(a)). This is a characteristic outcome of adsorbed electroactive redox couples [46], confirming that **ITO:4** behaves as an electrode with an attached redox couple. In this case, the expression for the current peak is:

$$i_{peak} = \left(\frac{n^2F^2}{4RT}\right) vA\Gamma^* \qquad (1)$$

where Γ^* is the total adsorbed amount of the redox-active species; n is the number of electrons per oxidized/reduced molecule; v is the potential scan rate and A is the geometric area of the electrode. F, R and T are the Faraday constant, universal gas constant and absolute temperature, respectively. This expression is obtained considering that both the oxidized and the reduced species are strongly adsorbed, a reversible charge transfer and a Langmuir-type isotherm describe the adsorption processes (ideal behaviour) [46–48] However, when charge transfer is quasi-reversible, the

$\frac{4RT}{n^2F^2vA\Gamma^*}i_{peak}$ ratio is not strictly equal to unity (see Fig. 2 in Ref. [49]). In the limiting case of the irreversible charge transfer, the expression for the peak current is then [49]:

$$i_{peak} = \left[4\alpha \exp\left(\frac{\kappa}{4\alpha} - 1\right)\right]\left(\frac{n^2F^2}{4RT}\right)vA\Gamma^* \approx 1.47\alpha\left(\frac{n^2F^2}{4RT}\right)vA\Gamma^* \quad (2)$$

where $\kappa = \frac{4RTk^0}{nFv}$, k^0 is the standard rate constant and α is the transfer coefficient by the forward scan in the Butler-Volmer-Erdey-Grúz equation [50,51].

By fitting the current-potential profiles obtained at different potential scan rates, using the model proposed by Myland and Oldham [49], $\kappa = 1.9$ $\left(\text{for } k^0 = 75\,\text{s}^{-1} \text{ and } v = 4.0\,\text{Vs}^{-1}\right)$ and the $\frac{4RT}{n^2F^2vA\Gamma^*}i_{peak} = 0.886$. This model does not consider lateral interactions between the adsorbed oxidized and reduced species [49].

The surface coverage (Γ^*) of **ITO:4** can be obtained from the linear fit of the data shown in in the inset of Fig. 2(a). The surface coverage calculated in this case was: $\Gamma^* = (1.4 \pm 0.1) \times 10^{-11}\,\text{mol cm}^{-2}$. This value is in good agreement with similar systems previously reported [45,52].

In a subsequent step, **ITO:4** substrates were exposed to more extreme potential sweep conditions for several cycles at different scan rates (5.000, 4.000, 2.000, 1.000 and 0.100 Vs^{-1}) and then again scanned at 5.000 Vs^{-1}. In Fig. 2(b), a decrease in current value is observed (blue line), suggesting the gradual loss of material, or its redox activity, at longer experimental times. The larger cathodic and anodic potential limits used in this case (-0.6 to 1.7 V vs. Ag) are responsible for different surface electrochemical events that distress the stability and behaviour of the modified electrodes.

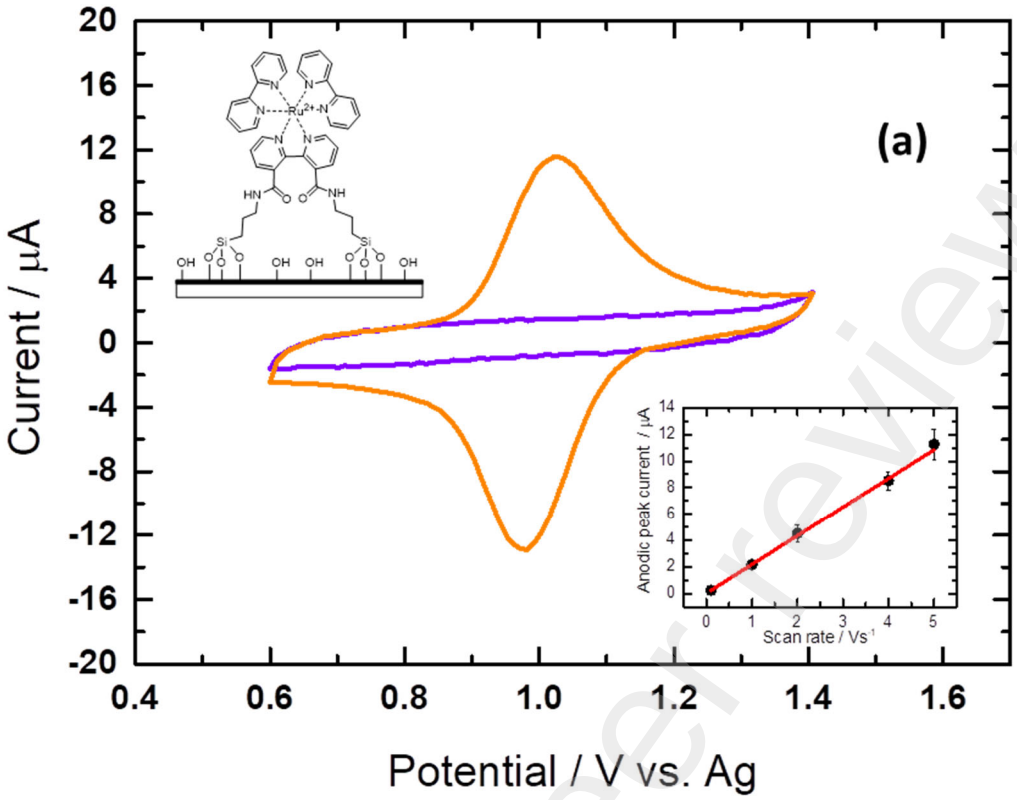

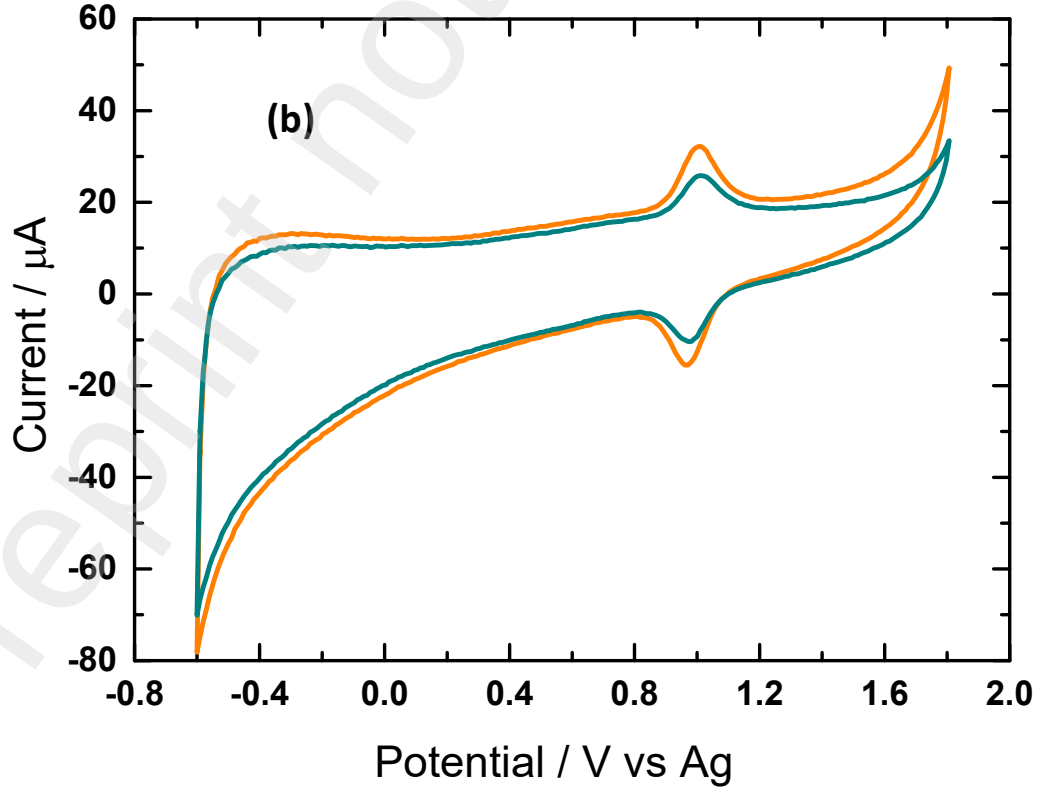

Figure 2: Cyclic voltammogram of **ITO:4** substrates (6th voltammetric cycle) (——) and bare ITO electrode (——) performed in 0.2 M H_2SO_4 at 5.000 Vs^{-1} **(a).** Anodic peak current as a function of scan rate (inset). Cyclic voltammogram of **ITO:4** substrates after 6th voltammetric cycles (——) and after several more cycles (——)**.** Experiments were performed in 0.2 M H_2SO_4 as electrolyte from -0.6 V to 1.7 V vs. Ag at 5.000 $V.s^{-1}$ **(b)**. Dipping conditions: solution of 0.5 mg mL^{-1} of **Complex 4** in 0.2 M H_2SO_4 for 30 minutes.

XPS measurements were used to identify the main changes in chemical composition between activated bare ITO substrates and the surface functionalized with **Complex 4** before and after electrochemical measurements. In Fig. 3, panels (a-c), the survey spectra are shown, highlighting the signals corresponding to the elements of interest. It can be observed that the RCA-treated ITO substrate has visible components of In3d, Sn3d, and O1s, typical expected features found in In-Sn oxide layer samples (Fig. 3 (a)). Also, the small N1s component indicates that there are no significant amounts of N atoms, an element presents in the RCA solution. Observing the Si 2p core-level region in detail, between 80 and 120 eV, the absence of signals indicates that the RCA treatment does not remove the ITO layer to expose the supporting silicate glass (Fig. 3 (a)). The comparison between bare and hydroxylated ITO (after treating with RCA) can be addressed in Fig. SI.1. (Supporting Information). On the other hand, XPS survey of sample **ITO:4** (Fig. 3 (b)) shows the presence of Si2p and Ru3d features together, suggesting the presence of **Complex 4** on the surface. It should be noted that the Ru3p signals are not visible, as seen in the XPS survey of Complex **3**, because this doublet overlaps with the Sn3d signals. The C1s/Ru3d core-levels analysis determine only one pair of Ru 3d signals for this sample (Ru3p 5/2 at 281.2 eV). The observation of Ru 3d signal coupled with C1s feature by XPS measurements of Ru-complex adsorbed on different conductive surfaces were also described in refs. [33,53,54]. The fact that the sample **ITO:4** contains only one pair of Ru 3d signal, unlike the two pairs obtained for the **Complex 4** (Fig. 1 (d)), suggests that Complex **3** is washed out when **ITO:4** substrate is formed. **Complex 4** has organosilane groups capable of binding to the surface of hydroxylated ITO during immersion [55], while Complex **3** does not have this ability and can be eliminated in the final washing of **ITO:4** substrate. Moreover, the electrochemical behaviour of ITO electrodes immersed in a solution containing only Complex **3** and then measured in the same electrolyte do not present an absorbed-type electrochemical signal.

After successive electrochemical measurements of **ITO:4** substrate in the larger potential window applied in this work (-0.5 to 1.7 V vs Ag), XPS survey and C1s/Ru3d region were

analysed. Although the survey spectrum appears similar (Fig. 3 (b) and (c)) to the one before cycling at first glance, a decrease of ~30% in the Si2p and Ru3d signals can be observed. It can be remarked that this effect is in agreement with the decrease in the current of the redox couple, observed by cyclic voltammetry, after successive potential sweeps in the same potential window as it was shown in Fig. 2 (b).

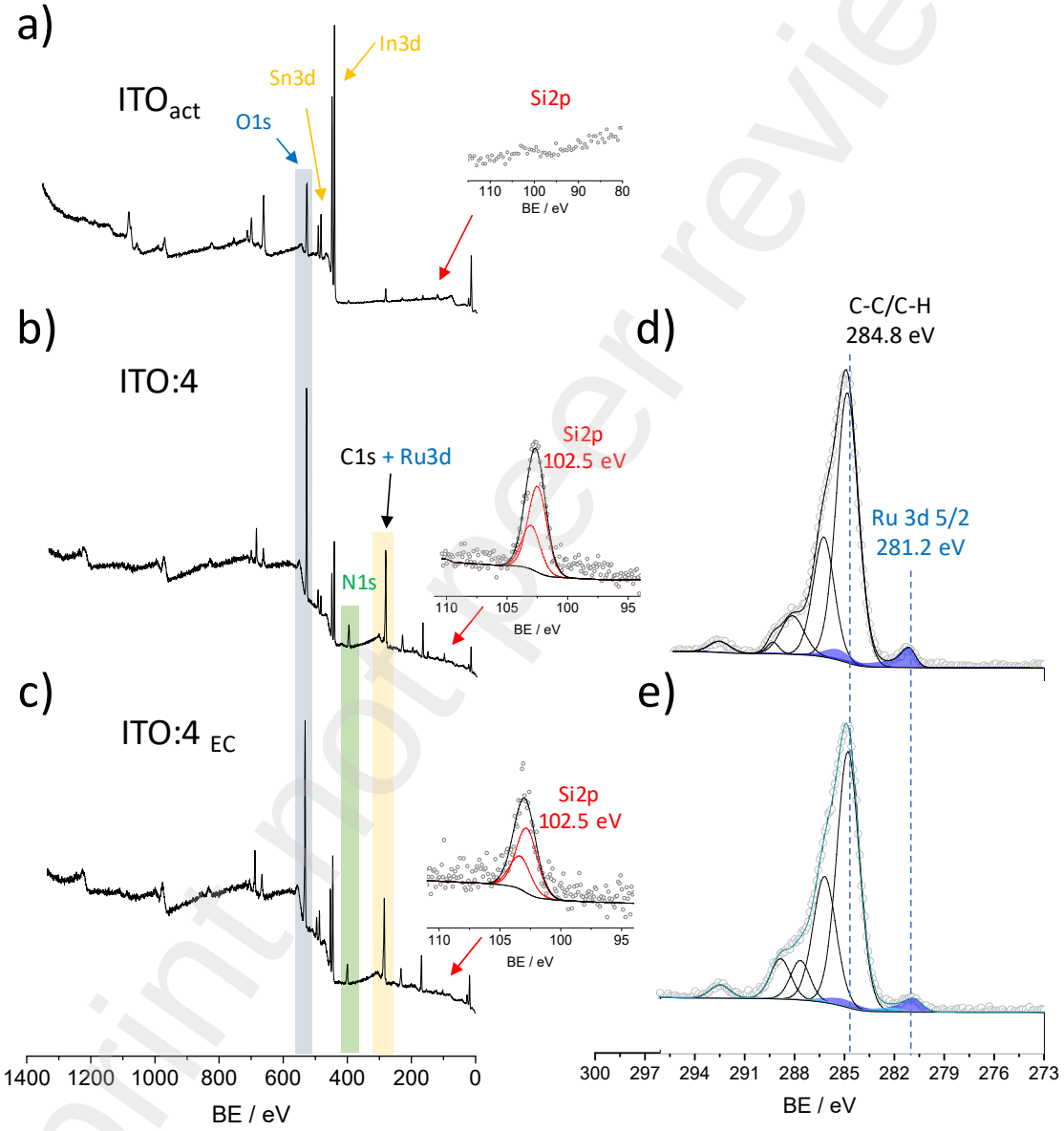

Figure 3: Survey spectra of activated ITO (a), **ITO:4** (b) and **ITO:4** after cycling (c). XPS C1s-Ru3d core-level of **ITO:4** (d) and **ITO:4** after cycling (e). Dipping conditions are the same as in Fig. 2.

3.5 Electrogenerated chemiluminescence (ECL)

Focusing on the co-reactant approach, TPA was introduced into the system as a co-reactant, while **Complex 4** was immobilized onto the ITO surface as a luminophore. Fig. 4 a) illustrates the experimental setup to generate an ECL signal. Fig. 4b) depicts the current-time profiles for the modified electrode (**ITO:4**) both in the absence and presence of 1.00 mM TPA in acetonitrile. The initial ECL signal started at potentials where the direct oxidation of TPA at the ITO electrode preceding the oxidation of immobilized **Complex 4**. It is evident that there exists a temporal correlation between the ECL signal and the oxidation currents of the ruthenium organosilane complex and TPA. This indicates that **Complex 4**, immobilized onto the ITO surface, retains its (electro)luminescent properties, and the concerted oxidation processes of **Complex 4** and TPA take place within the appropriate potential range.

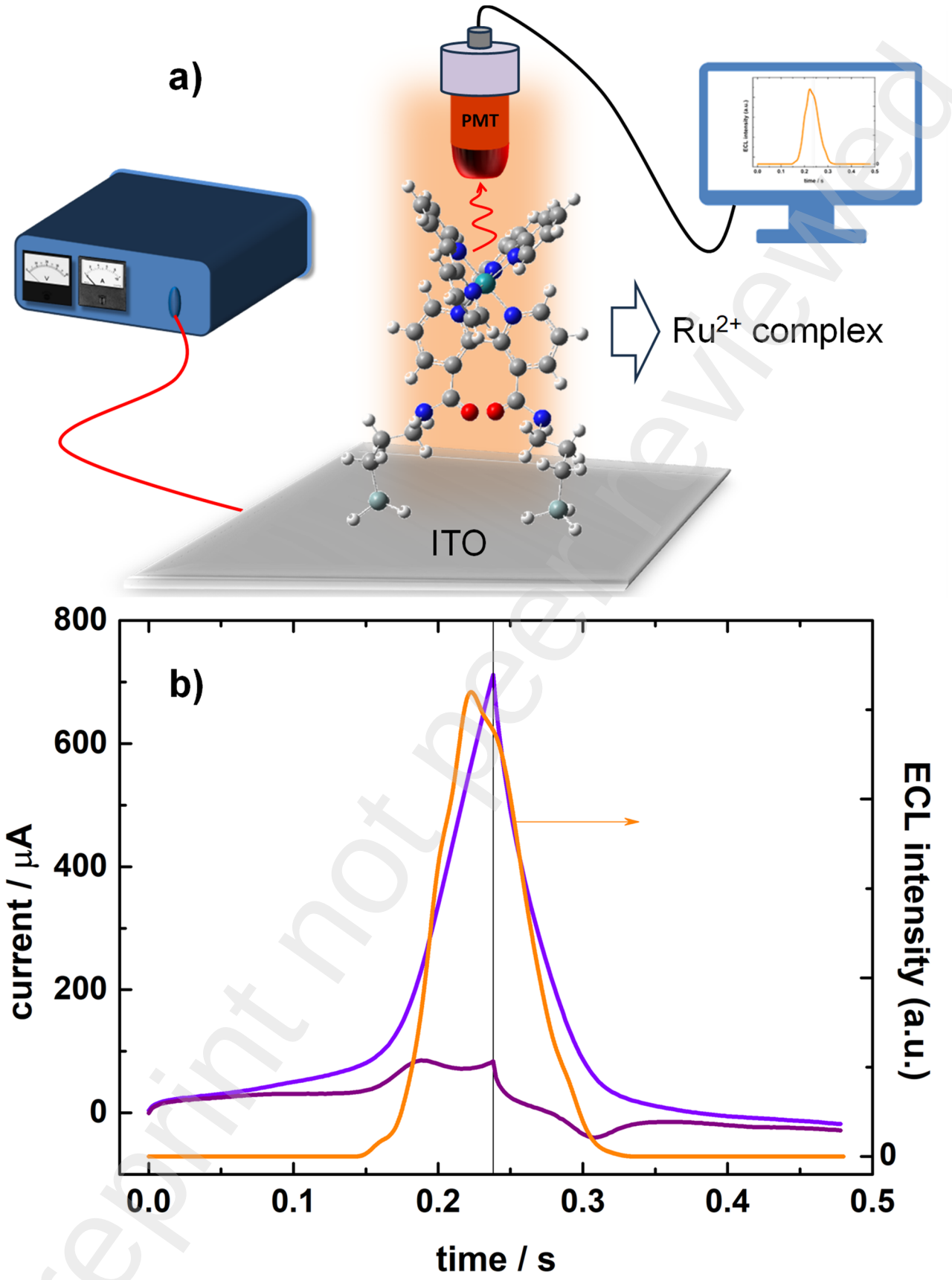

Figure 4. Scheme of the experimental array used for the ECL measurement (a) and current-time profiles of **ITO:4** substrates performed in 0.1 M $NaClO_4$ in acetonitrile at 5.000 Vs^{-1} b) 6th voltammetric cycles for **ITO:4** (——) and

ITO:4 + 1.00 mM TPA (——). Electrogenerated chemiluminescence obtained by **ITO:4** + 1.00 mM TPA (——). Dipping conditions are the same as in Fig. 2 (a).

4. Conclusion

An organic light-emitting compound with the capability to covalently bind to the surface of a transparent ITO conductor has been successfully synthesized. This compound comprises a ruthenium (II) complex with two molecules of bipyridine and a third modified bipyridine molecule containing organosilane groups, facilitating its covalent attachment to the ITO surface. Elemental analysis and chemical structure examination via XPS confirmed the covalent bonding of the modified ruthenium complex to ITO through its surface hydroxylated functionalities. Additionally, electrochemical experiments confirmed the presence of a redox couple attached to the surface, attributed to the Ru(III)/Ru(II) couple. A surface coverage of $(1.4 \pm 0.1) \times 10^{-11}$ mol cm^{-2}, consistent with similar systems [45,52], was obtained. The robustness of the substrate was assessed through successive electrochemical experiments, revealing a decrease in material content over extended experimental durations and wide potential windows.

The preliminary results of the ECL measurements, along with the surface properties of the modified substrates investigated in this study, are promising for the integration of modified electrodes with light-emitting materials to develop novel optoelectronic devices.

Acknowledgements

R.A.F; C.I.V, J.E.A; F.P.C. and S.A.D. are Researchers from Consejo Nacional de Investigaciones Científicas y Técnicas (CONICET). F.M. thanks CONICET for the fellowship granted. Financial support from CONICET (PUE: 22920160100013CO-INFIQC and PIP 11220210100666CO) and Secretaría de Ciencia y Tecnología de la Universidad Nacional de Córdoba - SECyT-UNC (33620180100677CB) are gratefully acknowledged.

References

[1] A.J. Bard, ed., Electrogenerated Chemiluminescence, Marcel Dekker, New York, 2004. https://doi.org/10.1016/s1522-5720(05)70074-x.

[2] N. Sojic, ed., Analytical Electrogenerated Chemiluminescence. From Fundamentals to Bioassays, Royal Society of Chemistry, Cambridge, UK, 2020. https://doi.org/10.1039/9781788015776.

[3] J.K. Leland, M.J. Powell, Electrogenerated Chemiluminescence: An Oxidative-Reduction Type ECL Reaction Sequence Using Tripropyl Amine, J. Electrochem. Soc. 137 (1990) 3127–3131. https://doi.org/10.1149/1.2086171.

[4] M.M. Richter, Electrochemiluminescence (ECL), Chem. Rev. 104 (2004) 3003–3036.

[5] R.J. Forster, P. Bertoncello, T.E. Keyes, Electrogenerated chemiluminescence, Annu. Rev. Anal. Chem. 2 (2009) 359–385. https://doi.org/10.1146/annurev-anchem-060908-155305.

[6] N.E. Tokel-Takvoryan, R.E. Hemingway, A.J. Bard, Electrogenerated Chemiluminescence. XIII. Electrochemical and Electrogenerated Chemiluminescence Studiesm of Ruthenium Chelates, J. Am. Chem. Soc. 95 (1973) 6582–6589. https://doi.org/10.1021/ja00801a011.

[7] S. Workman, M.M. Richter, The effects of nonionic surfactants on the Tris(2,2'-bipyridyl)ruthenium(II)-tripropylamine electrochemiluminescence system, Anal. Chem. 72 (2000) 5556–5561. https://doi.org/10.1021/ac000800s.

[8] W. Miao, J. Choi, A.J. Bard, Electrogenerated Chemiluminescence 69 : The Tri-n-propylamine (TPrA) System Revisited s A New Route Involving TPrA • + Cation Radicals, J. Am. Chem. Soc. (2002) 14478–14485.

[9] W. Miao, Electrogenerated Chemiluminescence and Its Biorelated Applications, Chem. Rev. 39 (2008) 2506–2553. https://doi.org/10.1002/chin.200841260.

[10] Z. Chen, Y. Zu, Electrogenerated chemiluminescence of the tris(2,2′-bipyridine) ruthenium(II)/tri-n-propylamine (TPrA) system: Crucial role of the long lifetime of TPrA+ cation radicals suggested by electrode surface effects, J. Phys. Chem. C. 112 (2008) 16663–16667. https://doi.org/10.1021/jp802873e.

[11] G. Valenti, A. Fiorani, H. Li, N. Sojic, F. Paolucci, Essential Role of Electrode Materials in Electrochemiluminescence Applications, ChemElectroChem. 3 (2016) 1990–1997. https://doi.org/10.1002/celc.201600602.

[12] A. Zanut, A. Fiorani, S. Rebeccani, S. Kesarkar, G. Valenti, Electrochemiluminescence as emerging microscopy techniques, Anal. Bioanal. Chem. 411 (2019) 4375–4382. https://doi.org/10.1007/s00216-019-01761-x.

[13] A. Zanut, A. Fiorani, S. Canola, T. Saito, N. Ziebart, S. Rapino, S. Rebeccani, A. Barbon, T. Irie, H.P. Josel, F. Negri, M. Marcaccio, M. Windfuhr, K. Imai, G. Valenti, F. Paolucci, Insights into the mechanism of coreactant electrochemiluminescence facilitating enhanced bioanalytical performance, Nat. Commun. 11 (2020) 1–9. https://doi.org/10.1038/s41467-020-16476-2.

[14] E. Kerr, E.H. Doeven, P.S. Francis, Recent advances in mechanistic understanding and analytical methodologies of the electrochemiluminescence of tris(2,2′-bipyridine)ruthenium(II) and tri-n-propylamine, Curr. Opin. Electrochem. 35 (2022) 101034.

https://doi.org/10.1016/j.coelec.2022.101034.

[15] F. Kanoufi, Y. Zu, A.J. Bard, Homogeneous oxidation of trialkylamines by metal complexes and its impact on electrogenerated chemiluminescence in the trialkylamine/Ru(bpy)32+ system, J. Phys. Chem. B. 105 (2001) 210–216. https://doi.org/10.1021/jp002880+.

[16] M. Singh, N. Kaur, E. Comini, The role of self-assembled monolayers in electronic devices, J. Mater. Chem. C. 8 (2020) 3938–3955. https://doi.org/10.1039/d0tc00388c.

[17] Y. Zu, A.J. Bard, Electrogenerated chemiluminescence. 66. The role of direct coreactant oxidation in the ruthenium tris(2,2')bipyridyl/tripropylamine system and the effect of halide ions on the emission intensity, Anal. Chem. 72 (2000) 3223–3232. https://doi.org/10.1021/ac000199y.

[18] N.E. Tokel, A.J. Bard, Electrogenerated Chemiluminescence. IX. Electrochemistry and Emission from Systems Containing Tris(2,2′-bipyridine)ruthenium(II) Dichloride, J. Am. Chem. Soc. 94 (1972) 2862–2863. https://doi.org/10.1021/ja00763a056.

[19] I. Rubinstein, A.J. Bard, Polymer Films on Electrodes. 4. Nafion-Coated Electrodes and Electrogenerated Chemiluminescence of Surface-Attached Ru(bpy)2+3, J. Am. Chem. Soc. 102 (1980) 6641–6642. https://doi.org/10.1021/ja00541a080.

[20] D. Ege, W.G. Becker, A.J. Bard, Electrogenerated Chemiluminescent Determination of Ru(bpy)32+ at Low Levels, Anal. Chem. 56 (1984) 2413–2417. https://doi.org/10.1021/ac00277a036.

[21] X. Zhang, A.J. Bard, Electrogenerated chemiluminescent emission from an organized (L-B) monolayer of a Ru(bpy)32+-based surfactant on semiconductor and metal electrodes, J. Phys. Chem. 92 (1988) 5566–5569. https://doi.org/10.1021/j100331a007.

[22] Y.S. Obeng, A.J. Bard, Electrogenerate Chemiluminescence. 53. Electrochemistry and Emission from Adsorbed Monolayers of a Tris (bipyridyl) ruthenium (II) -Based Surfactant on Gold and Tin Oxide Electrodes, Langmuir. 7 (1991) 195–201.

[23] P. McCord, A.J. Bard, C.J. Miller, Study of Langmuir Monolayers of Ruthenium Complexes and Their Aggregation by Electrogenerated Chemiluminescence, Langmuir. 7 (1991) 2781–2787. https://doi.org/10.1021/la00059a061.

[24] Y. Zu, A.J. Bard, Dependence of Light Emission of the Tris (2 , 2 ′) bipyridylruthenium (II)/ Tripropylamine System on Electrode Surface Hydrophobicity, Anal. Chem. 73 (2001) 3960–3964.

[25] H. Wei, E. Wang, Solid-state electrochemiluminescence of tris(2,2′-bipyridyl) ruthenium, TrAC - Trends Anal. Chem. 27 (2008) 447–459. https://doi.org/10.1016/j.trac.2008.02.009.

[26] H. Wei, E. Wang, Electrochemiluminescence of tris(2,2′-bipyridyl)ruthenium and its applications in bioanalysis: A review, Luminescence. 26 (2011) 77–85.

https://doi.org/10.1002/bio.1279.

[27] G.M. Greenway, A. Greenwood, P. Watts, C. Wiles, Solid-supported chemiluminescence and electrogenerated chemiluminescence based on a tris(2,2′-bipyridyl)ruthenium(II) derivative, Chem. Commun. 44 (2006) 85–87. https://doi.org/10.1039/b511071h.

[28] H. Wei, Y. Du, J. Kang, E. Wang, Label free electrochemiluminescence protocol for sensitive DNA detection with a tris(2,2′-bipyridyl)ruthenium(II) modified electrode based on nucleic acid oxidation, Electrochem. Commun. 9 (2007) 1474–1479. https://doi.org/10.1016/j.elecom.2007.01.053.

[29] L. Zhang, Z. Xu, X. Sun, S. Dong, A novel alcohol dehydrogenase biosensor based on solid-state electrogenerated chemiluminescence by assembling dehydrogenase to Ru(bpy)32+-Au nanoparticles aggregates, Biosens. Bioelectron. 22 (2007) 1097–1100. https://doi.org/10.1016/j.bios.2006.03.026.

[30] X. Wang, P. Dong, W. Yun, Y. Xu, P. He, Y. Fang, A solid-state electrochemiluminescence biosensing switch for detection of thrombin based on ferrocene-labeled molecular beacon aptamer, Biosens. Bioelectron. 24 (2009) 3288–3292. https://doi.org/10.1016/j.bios.2009.04.019.

[31] F. Lupo, M.E. Fragalà, T. Gupta, A. Mamo, A. Aureliano, M. Bettinelli, A. Speghini, A. Gulino, Luminescence of a Ruthenium Complex Monolayer, Covalently Assembled on Silica Substrates, upon CO Exposure, J. Phys. Chem. C. 114 (2010) 13459–13464. https://doi.org/10.1021/jp1028917.

[32] T. Akiyama, M. Inoue, Y. Kuwahara, S. Yamada, Novel photoelectrochemical cell using a self-assembled monolayer of a ruthenium (II) tris(2,2′-bipyridine) thiol derivative, Japanese J. Appl. Physics, Part 1 Regul. Pap. Short Notes Rev. Pap. 41 (2002) 4737–4738. https://doi.org/10.1143/jjap.41.4737.

[33] M. Küllmer, P. Endres, S. Götz, A. Winter, U.S. Schubert, A. Turchanin, Solution-Based Self-Assembly and Stability of Ruthenium(II) Tris-bipyridyl Monolayers on Gold, ACS Appl. Mater. Interfaces. 13 (2021) 60544–60552. https://doi.org/10.1021/acsami.1c10989.

[34] A.M. Spehar-Délèze, S. Almadaghi, C.K. O'Sullivan, Development of solid-state electrochemiluminescence (ECL) sensor based on Ru(bpy)32+-encapsulated silica nanoparticles for the detection of biogenic polyamines, Chemosensors. 3 (2015) 178–189. https://doi.org/10.3390/chemosensors3020178.

[35] A.M. Andersson, R. Isovitsch, D. Miranda, S. Wadhwa, R.H. Schmehl, Electrogenerated chemiluminescence from Ru(II) bipyridylphosphonic acid complexes adsorbed to mesoporous TiO2/ITO electrodes, Chem. Commun. (2000) 505–506. https://doi.org/10.1039/a908148h.

[36] T. Shinomiya, H. Ozawa, Y. Mutoh, M.A. Haga, A redox-active porous coordination network film based on a Ru complex as a building block on an ITO electrode, Dalt. Trans. 42 (2013) 16166–16175. https://doi.org/10.1039/c3dt51484f.

[37] W. Kern, J. Vossen, eds., Thin Film Processes, Academic Press, New York, 1978.

[38] W. Kern, Evolution of silicon wafer cleaning technology, J. Electrochem. Soc. 90 (1990) 1887–1892. https://doi.org/10.1149/1.2086825.

[39] B.K. Kanungo, M. Baral, S. Bhattacharya, Y. Sahoo, Synthesis of new macrocycles with 2,2′-bipyridyl and polyamine functions, Synth. Commun. 33 (2003) 3159–3164. https://doi.org/10.1081/SCC-120023436.

[40] H. Yang, H. Gao, R.J. Angelici, S.D. Brown, T.G. Richmond, Hydrodefluorination of fluorobenzene and 1,2-difluorobenzene under mild conditions over rhodium pyridylphosphine and bipyridyl complexes tethered on a silica-supported palladium catalyst, Organometallics. 13 (2000) 134–138.

[41] B.P. Sullivan, D.J. Salmon, T.J. Meyer, Out By Slow Evaporation of an Ether-Acetone Solution ., Inorg. Chem. 17 (1978) 3334–3341.

[42] B. Robert, V. Flaud, R. Escalier, A. Mehdi, C. Vigreux, XPS study of Ge-Se-Te surfaces functionalized with organosilanes, Appl. Surf. Sci. 607 (2023) 154921. https://doi.org/10.1016/j.apsusc.2022.154921.

[43] D.J. Morgan, Resolving ruthenium: XPS studies of common ruthenium materials, Surf. Interface Anal. 47 (2015) 1072–1079. https://doi.org/10.1002/sia.5852.

[44] C. Donley, D. Dunphy, D. Paine, C. Carter, K. Nebesny, P. Lee, D. Alloway, N.R. Armstrong, Characterization of indium-tin oxide interfaces using X-ray photoelectron spectroscopy and redox processes of a chemisorbed probe molecule: Effect of surface pretreatment conditions, Langmuir. 18 (2002) 450–457. https://doi.org/10.1021/la011101t.

[45] W. Guo, Z. Cao, Y. Liu, B. Su, Electrochemiluminescence of a Vinyl-Functionalized Ruthenium Complex and Its Monolayer Formed through the Photoinduced Thiol-Ene Click Reaction, ChemElectroChem. 4 (2017) 1763–1767. https://doi.org/10.1002/celc.201600905.

[46] A.J. Bard, C.R. Faulkner, Electrochemical Methods, Fundamentals and Applications, Second Ed., John Wiley & Sons, New York, 2001.

[47] E. Laviron, General expression of the linear potential sweep voltammogram in the case of diffusionless electrochemical systems, J. Electroanal. Chem. 101 (1979) 19–28.

[48] M.J. Honeychurch, G.A. Rechnitz, Voltammetry of Adsorbed Molecules. Part 1: Irreversible Redox Systems, Electroanalysis. 10 (1998) 285–293. https://doi.org/10.1002/(SICI)1521-4109(199806)10:7<453::AID-ELAN453>3.0.CO;2-F.

[49] J.C. Myland, K.B. Oldham, Quasireversible cyclic voltammetry of a surface confined redox

system: A mathematical treatment, Electrochem. Commun. 7 (2005) 282–287. https://doi.org/10.1016/j.elecom.2005.01.005.

[50] J.A.V. Butler, STUDIES IN HETEROGENEOUS EQUILIBRIA. PART III. A KINETIC THEORY OF REVERSIBLE OXIDATION POTENTIALS AT INERT ELECTRODES., Trans. Faraday Soc. 19 (1924) 734–739.

[51] T. Erdey-Grúz, M. Volmer, Zur Theorie der Wasserstoff Überspannung, Zeitschrift Für Phys. Chemie. 150A (1930) 203–213. https://doi.org/10.1515/zpch-1930-15020.

[52] A.L. Eckermann, D.J. Feld, J.A. Shaw, T.J. Meade, Electrochemistry of redox-active self-assembled monolayers, Coord. Chem. Rev. 254 (2010) 1769–1802. https://doi.org/10.1016/j.ccr.2009.12.023.

[53] C. Agnès, J.C. Arnault, F. Omnès, B. Jousselme, M. Billon, G. Bidan, P. Mailley, XPS study of ruthenium tris-bipyridine electrografted from diazonium salt derivative on microcrystalline boron doped diamond, Phys. Chem. Chem. Phys. 11 (2009) 11647–11654. https://doi.org/10.1039/b912468c.

[54] M. Laurans, J.A.L. Wells, S. Ott, Immobilising molecular Ru complexes on a protective ultrathin oxide layer of p-Si electrodes towards photoelectrochemical CO2reduction, Dalt. Trans. 50 (2021) 10482–10492. https://doi.org/10.1039/d1dt01331a.

[55] M. Sypabekova, A. Hagemann, D. Rho, S. Kim, Review: 3-Aminopropyltriethoxysilane (APTES) Deposition Methods on Oxide Surfaces in Solution and Vapor Phases for Biosensing Applications, Biosensors. 13 (2023) 36. https://doi.org/10.3390/bios13010036.

Supporting Information

Synthesis of Compound 2

A mixture of 1,10-phenantroline (2.0 g, 10 mmol), NaOH (0.8 g, 20 mmol) and $KMnO_4$ (4.7 g, 30 mmol) were dissolved in 120 mL distilled water and reflux for 6 h with stirring. The brown precipitate obtained of MnO_2 was filtered off, while hot. The volume of the filtrate was reduced to approx. 50 mL on rotary evaporator. Concentrate HCl was added until get white crystals at pH 2-3. The solid was filtered off, washed with water and ethanol. The filtrate was collected, and the volume reduced to half and left at 5 ºC overnight while more crystals separated out. All crystals obtained are dried to obtain product 1, analysed by ^1H RMN [39]. A mixture of APTES (2.33 mL, 10 mmol), Compound **1** (1.46 g, 6 mmol) and DCC (3.1 g, 15 mmol) was taken in 190 mL acetonitrile, under Ar atmosphere, and heated with stirred at 50 ºC for 12 h. White solid of 1,3-Dicyclohexyl urea (DCU) was filtered off while hot and washed with ethanol. The filtrate was dried on rotary evaporator to obtain Compound **2** as orange yellow oil.

Synthesis of Complex 4

A mixture of commercial $RuCl_3 \cdot 3H_2O$ (0.5 g, 2 mmol), 2,2'-bipyridine (0.6 g, 4 mmol) and LiCl (0.25 g, 6 mmol) were dissolved in 5 mL of dimethylformamide and reflux for 8 h with stirring. After the reaction mixture was cooled to room temperature, 15 mL of acetone was added, and the resultant solution cooled at 0 ºC overnight. The obtained black crystals of Complex **3** was filtered off, washed with water and diethylether and dried. The red-violet filtrate was reduced to half and left at 0 ºC over-night until more crystals came out. Finally, Complex **3** (0.48 g, 1 mmol) and Compound **2** (0.65 g, 1 mmol) were dissolved in 35 mL of absolute ethanol and heated at 50 ºC for 48 h with stirring. Ethanol was filtered off and the product was recrystallized from hot acetone, to obtain **Complex 4** as red-brown solid.

Mass spectrometry of the synthesised compounds.

In Fig. SI.1 (a-b), mass spectra of the synthesised compounds are shown. A main signal is observed around 532 m/z corresponding to molecular weight of the expected complex. The ion with 532 m/z can be assigned to **Complex 4** after loss two Cl^- counteranions with its characteristic Ruthenium isotopic mass distribution as can be observed. In Fig. SI.1(b), a peak at 651 m/z corresponds to Compound **2** [M+H], while the signal at 430 m/z can be attributed to a loss of an APTES molecule from the Compound **2** due to sample ionization during the measurement.

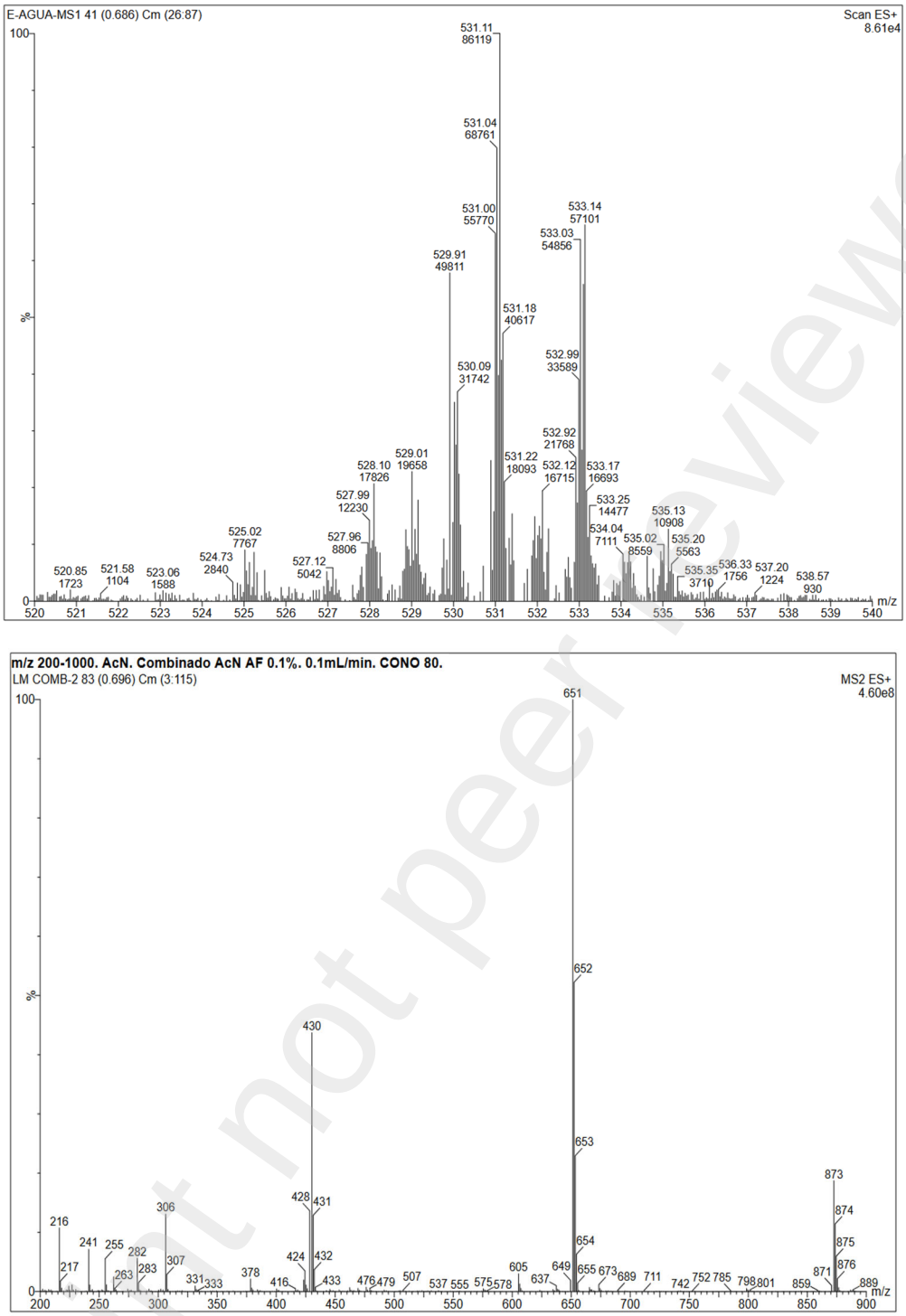

Figure SI.1: Mass spectrometry of synthetized products. **Complex 4** (a) and Compound **2** (b).

XPS measurements of the changes of the ITO surface after activation.

In order to determine the effectiveness of the ITO activation after RCA treatment [37,38], we performed XPS measurements. In Fig. SI.2 shows the O 1s spectra of ITO sample before and after treatment. It is shown that peak the peak at 532 eV attributed to the OH species increases after treatment.

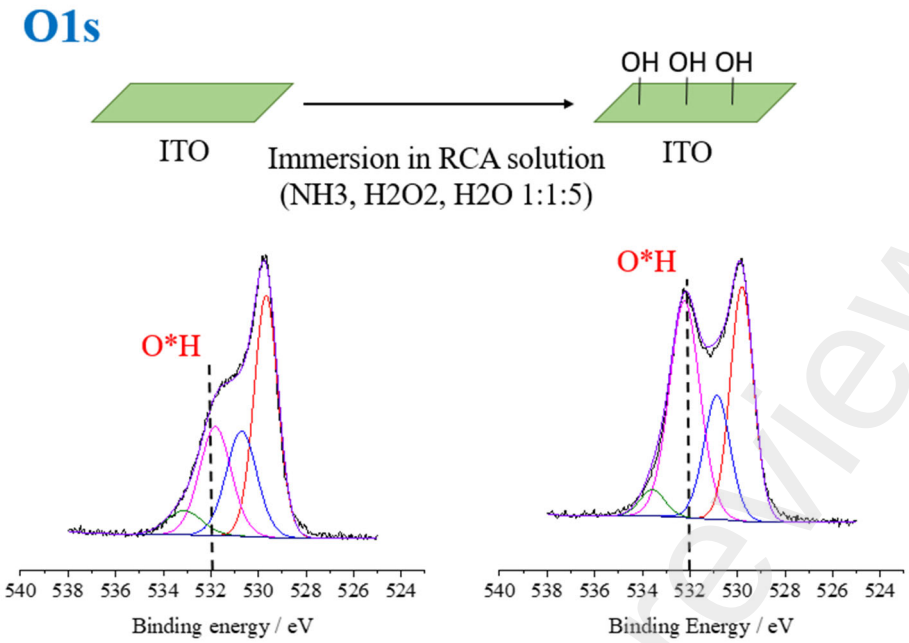

Figure SI.2: O1s XPS spectra of ITO surface before (left) and after (right) RCA treatment.